AUTHOR(S): PRATHURU, A.K., FAISAL, N.H., JIHAN, S., STEEL, J.A. and NJUGUNA, J.

TITLE: Stress analysis at the interface of metal-to-metal adhesively bonded joints subjected to 4-point bending: finite element method.

YEAR: 2017

Publisher citation: PRATHURU, A.K., FAISAL, N.H., JIHAN, S., STEEL, J.A. and NJUGUNA, J. 2017. Stress analysis at the interface of metal-to-metal adhesively bonded joints subjected to 4-point bending: finite element method. Journal of adhesion [online], 93(11), pages 855-878. Available from: https://dx.doi.org/10.1080/00218464.2016.1172309

OpenAIR citation: PRATHURU, A.K., FAISAL, N.H., JIHAN, S., STEEL, J.A. and NJUGUNA, J. 2017. Stress analysis at the interface of metal-to-metal adhesively bonded joints subjected to 4-point bending: finite element method. Journal of adhesion, 93(11), pages 855-878. Held on OpenAIR [online]. Available from: https://dx.doi.org/10.1080/00218464.2016.1172309

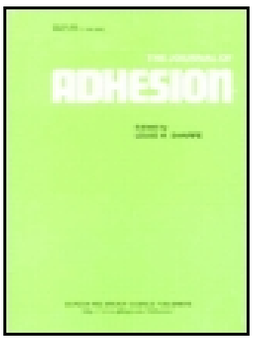

The Journal of Adhesion

ISSN: 0021-8464 (Print) 1545-5823 (Online) Journal homepage: http://www.tandfonline.com/loi/gadh20

Stress analysis at the interface of metal-to-metal adhesively bonded joints subjected to 4-point bending: Finite element method

Anil K. Prathuru, Nadimul H. Faisal, Sha Jihan, John A. Steel & James Njuguna

To cite this article: Anil K. Prathuru, Nadimul H. Faisal, Sha Jihan, John A. Steel & James Njuguna (2016): Stress analysis at the interface of metal-to-metal adhesively bonded joints subjected to 4-point bending: Finite element method, The Journal of Adhesion, DOI: 10.1080/00218464.2016.1172309

To link to this article: http://dx.doi.org/10.1080/00218464.2016.1172309

Accepted author version posted online: 12 Apr 2016.

Stress analysis at the interface of metal-to-metal adhesively bonded joints subjected to 4-point bending: Finite element method

Anil K. Prathuru, Nadimul H. Faisal[1], Sha Jihan, John A. Steel, James Njuguna

School of Engineering, Robert Gordon University, Garthdee Road, Aberdeen, AB10 7GJ, UK

Abstract

This paper presents a study of stress states in two-dimensional models of metal-to-metal adhesively bonded joints subjected to 4-point flexural loading using finite element (FE) method. The FE simulations were carried out on adhesive bonded joints of high support span to specimen thickness ratio undergoing extensive plastic deformations. Two different adhesive types with eight different adhesive layer thicknesses each varied between 50 μm to1500 μm were considered. The lower interfaces in the brittle adhesive were observed to be under a lower stress state because of the constraint exerted by a relatively stiff lower adherend. The ductile adhesive layers were under a lower state of stress as a result of the lower elastic modulus. It is concluded that the degree of plastic deformation in the adhesive is dictated by the adherend stiffness and the load transfer along the interface. The effect of load and support pins is noticeable at all adhesive thicknesses. High stress localisation exists in the vicinity of the load pins. The constraint exerted by the adherends dictates the deformation gradient through thickness of the adhesive layer. Adhesive joint behaviour as determined by the adhesive properties are investigated and also

[1] Author to whom correspondence should be addressed; E-mail: N.H.Faisal@rgu.ac.uk; Tel: +44-1224-26 2438

experimentally validated. Conclusions were drawn by correlating the adhesive and adherend stress states.

Keywords: finite element; 4-point bending; metal-to-metal adhesives; two-dimensional model; bending stress; adhesive joints

Notation

a : Distance of the load point from the support

d_m : Damage parameter

E : Elastic modulus

G_a : Specific energy of adhesion

G_c : Cohesive fracture energy

G_n : Normal energy release rate

G_{nc} : Normal energy release rate (critical value)

G_t : Tangential energy release rate

G_{tc} : Tangential energy release rate (critical value)

I : Second moment of the cross sectional area

K_m : Stiffness of the interface

L : Span length between supports

l : Specimen total length

P : Load

t : Adherend thickness

U_m : Mixed mode displacement

x : Distance of the section considered from one of the supports

$\acute{}$: Displacement

δ_c^m : Critical mixed-mode displacement beyond which the crack opens

σ_c^m : Critical stress (maximum traction)

$\tilde{A}_0$: Tensile strength of the brittle adhesive

$\tilde{A}_y$: Yield strength of the ductile adhesive

$\tilde{A}_t$: Shear strength of the brittle adhesive

$\tilde{A}_{td}$: Shear strength of the ductile adhesive

$\mathring{A}$: Poisson's ratio

APDL : ANSYS Parametric Design Language

FE : Finite Element

UDL : Uniformly Distributed Load

UTM : Universal Testing Machine

OA : Interface between lower adherend and adhesive

OB : Layer along mid-thickness of the adhesive

OC : Interface between upper adherend and adhesive

XX' : Axis of symmetry

1. Introduction

Recent advances in adhesively bonded materials have let design engineers meet structural integrity and higher strength requirements (e.g. oil and chemical processing industry aerospace or nuclear industries). They provide high strength-to-weight ratios, and are ideal for use with thin adherends which are likely choices for weight critical applications such as aircraft fuselage skin-stringer joints and wing-honeycomb core bonding etc. In most of these applications, the metal sheet thickness ranges from 0.6 mm to 1 mm [1]. Hence, predicting the failure mechanisms and loads of such bonded structures becomes important under various mechanical loading conditions. The quantification of adhesive bond strength as a function of various physical properties of the adhesive layer and adherends and the geometrical properties of the joint as a whole is highly affected by the level of constraint exerted by the adherends. The behaviour of the bond under various loading conditions depends to a large extent on the deformation in the adherends. It may

so happen that the adherends might yield even before any discernible failure occurs in the adhesive layer. Even though such behaviour is desirable, there still exists a need to predict the load carrying capability of such joints where high plastic deformation of the adherends is expected. The 4-point flexure loading is unique in a way that the span between the loading points is under a constant bending moment with no shear. Moreover, studies related to flexure testing of adhesive joints are minimal.

A study of single lap joints subjected to 4-point loading configuration was conducted by Karachalios *et al.* [2] with a uniform thickness of the adhesive layer. The study revealed a failure mechanism with cracks initiating at the tension side corner of the overlap length perpendicular to the principal stress direction and propagating through the adhesive layer. The shape and propagation of the cracks were significantly affected by the anticlastic bending along the width of the adherends. Similarly, Grant *et al.* [3] studied the failure of 3-, 4-point and tensile loaded single-lap joints. The joints tested in 4-point bending revealed no failure in the adhesive because of the yielding of the adherends at the loading points. A FE analytical comparison of 3- and 4-point bend tests of unidirectional composites done by Cui and Wisnom [4] revealed a higher damage of the composite under the loading roller in three-point loading. They reported a decrease of transverse compressive and tensile stresses by a factor of 20% under 4-point loading compared to 3-point loading. They also reported a decrease of 20% in the bending stresses when the non-linearity of the materials is considered. The study by Xie and Adams [5] concentrates on the shear testing of composite materials using 3- and 4-point flexural testing. FE and analytical methods were implemented to calculate the shear stress distributions in the composite laminates. The dependence of adhesive-laminar shear strength on the chosen support span length to

specimen thickness ratio has been reported. Feraboli and Edward [6] conducted a similar FE analysis on uni- and multi-directional composites of a constant span to thickness ratio subjected to 4-point loading configuration. The delamination has been reported to initiate at a small distance from the loading roller causing inter-laminar failure. Similarly, the mode-III failure of carbon/epoxy laminate has been studied by de Morais and Pereira [7] by subjecting them to a 4-point flexure loading. They implemented FE modelling in combination with cohesive zone modelling (CZM).

The behaviour of stepped lap joints under flexure loading has been studied by Sawa *et al.* [8] using FE method. In this case the axis of the bending load is perpendicular to the plane of the adhesive at the edges where failure initiates. The preliminary analysis of a single lap joint under 4-point bend loading has been set forth by Liu *et al.* [9]. They studied single lap joints with dissimilar adherends under flexure loadings. They concluded that the adherend thickness affects the stress state in the adhesive layer. Joints with thinner adherends tend to fail earlier. The 3-point flexure loading of adhesive joints has been studied by some researchers [e.g. 10]. The span to thickness ratio should be considered while deciding on the geometry of any adhesive joint test specimen as at lower span-thickness ratios, Saint Venant effects become considerably high. The volume around the loading points deforms and highly distorts the expected results thus rendering the specimen invalid. Hence, the size of the specimen should be chosen so as to allow sufficient volume for the load induced distortion.

The principal motivation of this study has been to understand the behaviour of slender adhesive joints under 4-point flexural loading. This loading condition has been chosen as the studies

related to it are quite few. Moreover, adhesive joints with high span-thickness ratio have been studied quite minimally. The FE simulations (including some experimental validation) were carried out on joints of high span to thickness ratio undergoing extensive plastic deformations for two different adhesive types (polyamide based brittle and acrylic based ductile adhesives). The stress distributions in the adhesive layer and the effect of loading conditions were analysed in detail. The effect of varying the adhesive thicknesses and properties were studied and the through-thickness stress distributions were investigated.

2. Finite element modelling and simulations

Figure 1a shows a model of an adhesively bonded metallic joint (e.g. aluminium, often selected for use where weight is critical) with an adhesive thickness under the 4-point flexural loading condition. The present analysis can be useful to understand the out of plane bending of the bonded zone of a simple lap-joint geometry and panel bonding. The Cartesian coordinate system was used with the origin at section XX2(**Figs. 1a** and **1b**). Two-dimensional (2D) FE simulations were done using ANSYS (14.0) Mechanical APDL package. The behaviour of both the adherends and the adhesive layer were modelled using a simple bi-linear law embedded in the package. This law models the plasticity of the isotropic materials as a straight line**;** the slope of which determines the hardening of the material after yield. Two different adhesives ratio were considered (**Table 1**, with relevant data cited from [8, 11, 12]). Eight different thicknesses of the adhesive layer were varied (50 µm, 100 µm, 250 µm, 500 µm, 750 µm, 1000 µm, 1250 µm and 1500 µm).

The dimensions and properties of the adherends and adhesives are shown in **Table 1** and the geometrical parameters are schematically represented in **Fig. 1a**. The dimensions of the adherends were chosen to understand the effect of adherend thickness and plastic deformation on the adhesive layer stress states. The study focuses on this aspect and endeavours to explain this in context of varying adhesive layer thickness for the two types of adhesives. Only half of the entire model has been considered because of symmetry of the load and support configurations. Both the adherends and the adhesive interlayers were meshed using PLANE 182 elements with plane-strain option. The sample mesh is shown in **Fig. 1b**. The element size was maintained at 5 μm (finer size) [9] along the thickness of the adhesive layer. The loading and support pins are modelled as rigid semi-circular bodies with radii of 2 mm (**Fig. 1c**). The rigidity of loading and support pins was attained by considering a very high elastic modulus value (100 times that of steel which has an elastic modulus of 210 GPa). Contact 172 and target 169 elements were used to model the contact between the adhesive joint, the load and support pins. These elements monitor the normal and frictional loads between the contact surfaces. The frictional co-efficient value of 0.2 was assumed between all contacting surfaces.

For all the models, a constant downward displacement boundary condition of 10 mm of the loading pin was applied which was constrained in the horizontal direction to prevent sliding on the upper adherend. The lower support was constrained in all directions. The adhesive was assumed to be perfectly bonded with the adherends at both the interfaces. The displacement increment in the solution stage was chosen to ensure a smooth loading of the model. Solution iterations were carried out until convergence was achieved. Convergence in this case was highly affected by the shift in the contact region between the joint, loading and support pins. To restrict

the solution instability caused by the frictional effects, program chosen time stepping was selected. This ensures sub-division of the load steps under highly unstable conditions.

Since the behaviour of the adhesive is the object of primary interest, various result items have been extracted along different paths parallel to the span along the thickness of the adhesive (namely OA, OB and OC) as shown in **Fig. 1d**. The 4-point bending model at the maximum displacement of 10 mm is shown in **Fig. 1e**. The nomenclature is same for all the thicknesses and the two types of adhesives considered in this study. In addition, the effect of the modulus mis-match on the adherend side of the interface was also observed. The total element and nodes employed in the calculations for 50 μm and 1500 μm thick adhesives are (3600, 4326) and (108000, 108871), respectively. 120 sampling data points were considered for result extraction along each path (OA, OB and OC, each 60 mm long). This number was optimised on the basis that the result contour does not change considerably even with a higher number of data points.

The stress results obtained were normalised with respect to the tensile strength ($\tilde{A}_0$) of the brittle adhesive and the yield strength ($\tilde{A}_y$) of the ductile adhesive (**Table 1**). To validate the 4-point bending, the FE model was implemented on a 2 mm thick aluminium (defined here as control specimen), and the elastic modulus calculated from the 4-point bending FE model using Equation 1 was 75 GPa, which is close to the literature value (elastic modulus of aluminium 68.4 GPa). It is important to note that the elastic modulus has been calculated for a plane strain condition and the literature value of elastic modulus has been taken for a plane stress condition (about 9% difference in this case). Plane strain condition has been chosen as the sandwich structures simulated is assumed to have high width to thickness ratio. The FE mesh was

optimised based on the validated elastic modulus value of aluminium and then the obtained optimised mesh was implemented in the adhesive joint model.

$$\delta = \frac{P(L-a)}{6LEI}\ \left[\frac{L}{L-a}\ (x-a)^3\text{-}x^3\ +\ (L^2\ \text{-}(L-a)^2\ )\ x\right] + \frac{Pa}{6LEI}\ \left[\frac{L}{a}\ (x-(L-a))^3\ \text{-}\ x^3\text{+}\ (L^2\text{-}a^2)\ x\right]$$

…… [1]

where ´ is the displacement, *P* is the load within the elastic limit, *L* is the span length between the supports, *a* is the distance of the load point from the support, *E* is the modulus of the material, *I* is the second moment of the cross sectional area (rectangular) and *x* is the distance of the section considered from one of the supports. In this case, since the FE model is two-dimensional, the load is considered per unit width and *I* is calculated accordingly.

Cohesive zone model (CZM) formulation: In addition to above FE formulation of the adhesive and the adherends, the interfaces between the two have been modelled using a cohesive zone model (CZM). It models the interfacial contact as a series of springs whose stiffness varies a function of the displacement. CONTACT 172 and TARGET 169 elements with de-bonding option have been created along the interface. The overall behaviour is represented by a traction-separation law whose shape determines the energy release rate during failure propagation. In this case, a triangular law has been implemented, as shown in **Fig. 2**. The parameters for the CZM have been determined by trial and error so as to match the experimental and simulation results. CZM's are based on the assumption that one or multiple fracture interfaces/regions can be artificially introduced in structures, in which damage growth is allowed by the introduction of a possible discontinuity in the displacement field. The technique consists on the establishment of traction-separation laws (addressed as CZM laws) to model interfaces or finite regions. The

CZM has been implemented only for the simulations with 250 μm brittle and ductile adhesive layers. The traction-separation relation is given by $P_m=K_mU_m(1-d_m)$, where 'd_m' is the damage parameter (a function of normal and tangential displacements which varies between 0 and 1, between δ_1^m and δ_c^m, respectively), 'K_m' is the initial stiffness of the interface, and 'U_m' is the mixed mode displacement. The fracture criterion is given by $\frac{G_n}{G_{nc}} + \frac{G_t}{G_{tc}}$ =1, where 'G_n' and 'G_t' are the normal and tangential energy release rates, and 'G_{nc}' and 'G_{tc}' are corresponding energy release rate critical values. As can be seen, the traction-displacement relation is represented by a triangle, the area of which is the steady-state fracture toughness of the interface. δ_c^m represents the critical mixed-mode displacement beyond which the crack opens. σ_c^m represents the critical stress and is the maximum traction the adhesive can sustain. CZM's are based on the concepts of stress and damage mechanics, and can be fitted into the local or continuum approach, since they can either be considered to model the interfacial fracture behaviour of equally or differently oriented plies in stacked composites or the adhesive/adherend interface to simulate adhesive failures (local approach), or on the other hand to simulate a thin bulk layer of a constant thickness material (continuum approach).

3. Experiments

Temper half-hard aluminium plates (AL000730, size: length 120 mm, width 50 mm and thickness 1.5 mm, and AL000645, size: length 120 mm, width 50 mm and thickness 0.5 mm; Goodfellow Cambridge Ltd., Huntingdon, UK) were selected for this study. The Vickers

microhardness of the 2 mm thick aluminium sheet was 37± 2 $HV_{1.96\ N\ (200\ g)}$ measured using HM 210A machine (Mitutoyo Ltd., Hampshire, UK).

Two types of adhesive bond materials (ductile bond: Loctite® 326™ [Henkel Ltd., Hemel Hempstead, UK], elastic modulus: 0.3 GPa [11]; brittle bond: Loctite® 3430™ [Henkel Ltd., Hemel Hempstead, UK], elastic modulus: 3.34 GPa [8]) were used between two aluminium plates (size: 120 mm × 50 mm; thicknesses 0.5 mm and 1.5 mm). **Figure 3** describes the scheme of the adhesive bond specimen preparation. As received aluminium metal plate surfaces were degreased using a surface cleaner (Loctite® 7063™ [Henkel Ltd., Hemel Hempstead, UK]) and then activator (Loctite® 7649™ [Henkel Ltd., Hemel Hempstead, UK]) was applied. The bond gap was controlled using thin aluminium shims, introduced to maintain a gap of 100 µm and 250 µm, respectively. The shims of very small size (2 mm x 1 mm each) and thicknesses 100 µm and 250 µm were adhesively bonded permanently to the lower plate at the four plate corners and at the centre of two 120 mm sides. These shims were adhesively bonded permanently in order to insure that they don't squeeze out during the application of uniform compressive pressure on top of the plate. The uniform distributed load (UDL) using known dead weights (20 N) was applied and specimens were cured for 24 hours.

The 4-point bending test apparatus (designed within the guideline of BS EN ISO 14125:1998) was assembled and experiments were carried out on adhesive bond specimen using 30 kN universal testing machine (Model 5567, Instron Ltd., High Wycombe, UK). The loading and support pins of radii of 2 mm was used. The specimens were tested with the thin adherend (0.5 mm) on top, the same set-up as investigated in FE simulation (in *Section 2*). The experiments

were displacement controlled with 2 mm per minute cross-head speed used in this study (with data sampled at 10 samples per second), and a total of two runs (4-point bending test) were investigated for each specimen. The force obtained from each test has been calculated per unit width of the specimen so as to be compared with the FE simulation force-displacement data.

4. Results and discussions

This work has two basic components, i.e. stress determination for the brittle and the ductile adhesives of various thicknesses that characterises the critical condition over the length of span. Each component will be discussed within the assumptions in the FE simulations. This section discusses the key results and outlines perspectives for future simulation and experimental work.

4.1 Effect of adhesive thickness and adherend deformation

An observation of the stress distribution plots shows that the span between the mid-axis and the load point is under more or less a uniform stress condition. There exists a considerable difference in the through thickness stress distribution between the 50 μm and 1500 μm thick adhesives (**Figs. 4a** and 4**b**). The path OA is at a lower stress state at higher thicknesses (e.g. **Fig. 4b** for 1500 μm thick adhesive) because of its association with the thicker (1.5 mm) adherend whose degree of plastic deformation being lower compared to the upper adherend (thinner, 0.5 mm). The adherends are known to have a constraining effect on the adhesive layer which is dependent on the modulus mis-match between the adherends and the adhesive and the adhesive thickness [13-16].

Tvergaad and Hutchinson [15] have investigated the effect of the adhesive layer thickness on the steady state toughness of an adhesive joint tested in Mode-I. They reported an increase in the toughness with an increase in the adhesive layer thickness with all the other parameters remaining constant. They attributed this behaviour to the elastic shielding of the adhesive layer at lower thicknesses. This constraining effect is due to the interaction of the stress field in the adhesive with the stiff adherends which modifies the shape and size of the plastic zone in the adhesive layer [10, 15, 17]. In the particular case of the brittle adhesive, this effect might further be assisted by its relatively higher stiffness (elastic modulus 11 times higher compared to ductile adhesive, **Table 1**) which confines the load to the upper layers. The term 'stiffness' has been used to refer to the deformability of the adhesive in this context implying the load-deformation behaviour of the adhesive. The variation of the stress between layers OA and OB (**Figs. 4c** and **4d**) can also be attributed to this combined effect (i.e. stiff lower adherend and brittle adhesive). Also, the distance of the layer concerned from the thicker (lower, 1.5 mm) adherend appears to affect the state of stress (i.e. the higher the distance, the higher is the stress state). The opposite can be said about the distance from the upper adherend due to the higher degree of plastic deformation because of its lower thickness. The increase in the adhesive thickness decreases the stress concentration because of higher degree of plastic deformation within the adhesive [10, 16].

Marzi *et al.* [16] reported an increase in the flexibility of adhesive joints with increasing adhesive thickness. The span along which higher stress states (stress higher than the compressive strength) can be seen, increases with increasing thicknesses along OB and OC (**Figs. 4d** and **4e)**. This is because of the distribution of the stress over a larger area with the increasing thickness. At lower thicknesses, the constraint of the adherends prevents the adhesive from straining to relieve the

stress from the high load-concentration point [16]. However, at higher thicknesses, restraint decreases, distributing the stress [13, 18]. A similar observation has been made by Xu *et al.* [19] that the increase in thickness increases the toughness by increasing the size of the plastic zone. The higher stress state along OC observed in all the simulations was probably because of two reasons: (a) OC is the upper interface (between the upper adherend and the adhesive), and (b) the upper adherend thickness is $1/3^{rd}$ of the lower adherend thickness and hence has undergone higher degree of plastic deformation which increases the degree of stress along the upper interface [13].

It is important to note that the X-directional stresses investigated here correspond to the in-plane tensile or compressive component. This particular component has been chosen instead of the Y-directional peel component as the failure was expected to occur within the adhesive layer because of the bending stress induced during loading. The contours of Y-directional stresses have also been studied but not presented in this manuscript as they are predominantly compressive within the sandwich structure and failure has not been deemed possible in such test configuration.

The shear stress distribution in the adhesive layers seems to be more or less uniform and close to zero along all the adhesive layer combinations simulated (**Figs. 5a to 5e**). This is consistent with the beam theory which states that there is no shear stress between the loading points in 4-point bending. However, at higher thicknesses of the adhesive layer, the shear stress exhibited a sharp decline from mid-span towards the load-pin location followed by high variations near the loading point since the shear stress is a result of the differential normal stress acting on the adhesive and

as the interface with the upper and lower adherends are subjected to higher stress variations due to localised loading at the load pins.

The stress concentration among the upper layers at higher thicknesses similar to brittle adhesive (discussed above) was not observed in the ductile adhesive (e.g. **Figs. 6c** and **6d**). The lower elastic modulus (of ductile adhesive) leads to a higher degree of deformation and strain transfer to the lower portions of the adhesive layer. Sawa *et al.* [8] reported a similar observation where in lower principal stresses were observed in ductile adhesive layers under combined tensile and bending loads. The similarity in the stress profiles for all the thicknesses can also be explained by the same. Even though the shear stress is consistently close to zero for all the thicknesses considered, the change in nature of the shear stress profiles for the various thicknesses of the ductile adhesive at the load point (e.g. **Figs. 7c** to **7e**) is attributed to the sudden change in the slope of the deflected beam at this location which induces a high degree of stress (and strain) concentration in the upper and lower adherends (i.e. lower adherend is under a high tensile strain at this point and the upper adherend is under a high compressive strain).

The increase in the adhesive thickness increases the load capacity of the joint (**Fig. 8a**). When compared to the ductile adhesive, the rate of increase of the load capacity with adhesive thickness is higher with brittle adhesive, though the difference is high only beyond a certain thickness. If the adhesive stress state is assumed to be a result of the relative deformation of the adherends, the load capacity increase with increasing adhesive layer thickness cannot be explained. The load increase with increasing thickness suggests that the adhesive layer has some load carrying capacity of its own and this is affected by the modulus of the adhesive.

4.2 Effect of adhesive modulus

The effect of the adhesive modulus can be seen in terms of the stress concentration and the degree of deformation along OA, OB and OC in the adhesive. A simple comparison of the stress state along path OA for the brittle and ductile adhesive s of similar thicknesses reveals interesting facts. As shown in **Fig. 9a**, the degree of stress concentration is considerably lower for the 50 μm ductile adhesive compared to the brittle adhesive. Similar trend can be seen (in **Fig. 9c**) with the shear stress distribution. However, for the 1500 μm thick adhesive layer, similar comparison (**Figs. 9b** and **9d**) shows that the difference between the brittle and ductile adhesives along the path OA is relatively less compared to that for the 50μm thick adhesive layer. This, as discussed, is a combined effect of the adhesive modulus and constraints because of the adherends [9, 16] and the adhesive layer thicknesses. From **Fig. 6c**, for the ductile adhesive, increase in the adhesive thickness does not show a significant effect on the stress distribution along OA (both the X-stress and shear stress), thus effectively showing the stress propagation from upper to lower interface in the ductile adhesive. The 4-point bending force-displacement profiles (**Fig. 8b**) show an increase in the stiffness of the joint with an increase in the adhesive interlayer thicknesses and at the same thickness, the stiffness increases with increasing modulus. The nature of the adhesive elastic modulus appears to have no effect on the force-displacement profile at an adhesive thickness of 50 μm (even beyond the elastic limit). The influence of the adherends appears to be dominant in this case and completely masks the relatively ductile nature of the adhesives.

From **Figs. 8a** and **8b**, the variation of load at the maximum displacement can be seen as a function of the adhesive layer thickness. It can be seen that at lower thicknesses, the adhesive joint with the brittle layer and the one with ductile layer have almost similar load carrying capabilities, irrespective of the adhesive modulus. This observation supports the claim that at lower adhesive layer thicknesses, the deformability of the adhesive layer and hence the flexibility of the joint are dictated by the adherend behaviour to a large extent. At higher adhesive layer thicknesses, the load carrying capacity is governed also by the adhesive material properties which can be seen as a higher load capacity at higher thicknesses of the brittle adhesive and also a larger difference in the load capacity of the brittle and ductile adhesive joints with similar adhesive layer thickness.

4.3 Peak stress variation in adhesive layer

Even though the stress variations along the span of the joint are quite high at specific locations (e.g. in the vicinity of the loading pin) because of St. Venant's effects, the overall distribution seems to follow a similar trend in all the geometries. The shear stresses are almost zero in the mid-span (XX´-loading pin) in the ductile adhesive and in the brittle adhesive the adherend plasticity has led to a slight deviation from this trend. The shear stress is believed to be induced by the relative motion of the adherends. The variation of the mid-span normalised von-Mises stress with the adhesive layer thickness is shown in the **Fig. 10a** and **Fig. 10b** for the brittle and ductile adhesives, respectively. The steady increase in the stress along the upper interface (OC) can be observed with increasing thickness until the stress crosses the yield point beyond which the entire upper interface can be assumed to have failed. The rate of increase of the mid-span

stress with the adhesive layer thickness decreases from the upper interface (OC) to lower interface (OA). A simple explanation of this behaviour has been investigated by looking at the joint as a composite beam under flexural load.

Fig. 11a and **Fig. 11b** show the position of OA, OB and OC with respect to the neutral axis of the composite beam with the brittle and ductile adhesives, respectively. The position of the neutral axis has been calculated according to simple beam theory. As can be seen, the peak mid-span von-Mises stress along the three layers follows a similar trend as the corresponding distance from the calculated neutral axis. The same behaviour can be seen in both the ductile and brittle adhesive layers, although the peak stresses in the ductile adhesive layers are quite low compared to those in the brittle adhesive.

4.4 Experimental validation of FE model of 4-point bending

Figure 12 shows experimental force-displacement profile for *Al*-to-*Al* adhesively bonded specimens with brittle (Loctite® 3430™ [Henkel Ltd., Hemel Hempstead, UK]) and ductile (Loctite® 326™ [Henkel Ltd., Hemel Hempstead, UK]) adhesives of thicknesses 100 µm and 250 µm and compares with corresponding FE model profile. It is important to note that the force (*y*-axis) obtained for each experiments (in **Fig. 12)** has been calculated per unit width (i.e. 50 mm) of the specimen to compare with the FE simulation force-displacement data. For a total displacement 10 mm, the features between specimen types (with brittle and ductile adhesive) in the force-displacement profile can be compared. There exists a good agreement between the experimental and FE simulation force-displacement profiles until the moderate stage of bending (e.g. within the elastic regime for 100 µm thick and both adhesives, **Fig. 12a**). However, for

thicker adhesive layer (e.g. within the elastic regime for 250 μm thick and both adhesives, **Fig. 12b**), the force-displacement profiles match well during the early stage of bending. The ductile adhesive bond fails at relatively higher load (at 4.5 N, i.e. abrupt change in the slope) compared to brittle adhesive bond which fails at about 3.5 N at very similar displacement. This is in contrast to the FE simulation and might be because of the inherent flaws in the adhesive bonded area which act as failure initiation locations early while loading. The abrupt change in the slope (i.e. sudden drop in the load) is referred here as a critical load (P_c) where large fracture/delamination has happened. For both bonded specimens with 100 μm thick adhesives (brittle and ductile, **Fig. 12a**), no such critical load was observed during the bending. However, for both bonded specimens, as the deflection ramps up further, the load attains a plateau. The failure in the 250 μm thick adhesive specimens occurred just as the specimen started exhibiting non-linear force-displacement behaviour. Since the load carrying capacity of the specimen depends on the metal plates, it can be inferred that the specimen failed as soon as the adherend yield initiated. Since the upper adherend in these specimens is thinner (0.5 mm), the degree of yield will be higher and hence the adhesive-adherend strain mismatch will be higher. Hence, the failure can be expected to occur in the vicinity of the upper adherend, which was the case in the failed specimens (**Fig. 12b**).

Overall, the differences between the experimental and FE simulation force-displacement profile are due to the assumptions of the FE model, the important one being the bi-linear modelling of the elastic-plastic nature of aluminium and the adhesives. The specimens with adhesive layer thickness of 250 μm exhibited failure in both specimens. This is seen as a sudden drop in the load during the test. However, the load kept steadily increasing even after failure because of the

load bearing capacity of the aluminium plates. As shown in **Fig. 12b**, the specimens with 250 μm thick adhesive layer appear to have failed as soon as the metal plates enter the plastic regime which is around the critical load in this particular case. Upon visual inspection of the failed specimens, the crack originated along the upper interface near the both load locations and travelled towards the centre of the span. This agrees with the predictions of the simulations, as discussed above in FE simulation sections. Also mentioned earlier, the FE simulations assumed that there exists a perfect bonding between the adhesive and the adherends along the interfaces and does not account for the existence of defects both within the adhesive and along the interface. Hence the failure of the specimen depends not only on the stress states within the adhesive layer but also on the presence of improper bonding (Kissing bonds), air bubbles, and foreign material inclusions, etc. The delamination along the upper interface could also be caused by the differential peel stress acting because of the stiffness difference between the lower and upper adherend.

In all these cases, the failure can be made to match experimental results very closely, by including additional constants. Constructing such specimens will require an increasing number of independent material parameters, which must all be best fitted by experiments. Apart from the amount of experimental work involved, this method does not help much to understand the physical failure mechanism of mixed mode fractures. Traditionally, CZM's have been used to represent the fracture behaviour of an entire adhesive layer, but in the present case, it has been utilised to represent the behaviour of just the adhesive-adherend interface in lines of the study conducted by Tvergaard and Hutchison [15]. This gives a reasonable idea of the interfacial delamination as well as the plastic deformation of the adhesive layer. In the present study, the

inclusion of CZM into the model for the 250 μm brittle and ductile adhesive layers has been taken up so as to simulate the weakening of the joint because of the presence of weak interfacial bonding. The CZM parameter set has been chosen so as to match the experimental and the simulation load-displacement profiles. This gives an idea of the effect of a weakened interface on the load carrying capability of an adhesive joint which by itself should explain the failure mechanisms.

In the experimental specimens tested for the 250 μm thick adhesive layer (**Fig. 12b**), failure was along the interface and this was primarily because of the high strain mis-match between the adhesive and the metal. The presence of manufacturing bond layer defects may also have led to localised stress concentrations and crack propagation by the agglomeration of these defects. Incorporation of these defects within the model will be the focus of future study. However, the agreement largely between the FE simulation and the experimental results validate the simulation technique.

4.5 Enhanced mechanical properties and measurements of bond quality

Practically, the adhesive bonds have heterogeneous structure, and bond delamination or cracking (adhesive or cohesive) often originates from micro-cracks or in-efficient bond strength between the mating (metal-adhesive-metal) surfaces. Since such adhesive bonds are employed in applications ranging from design and production to repair, maintenance, and field service, if the cracking propagates along the interface of adherend and adhesive (defined as specific adhesion energy, G_a) or within the (defined as cohesive fracture energy, G_c), it becomes apparent that a

combined simulation and experiment based characterisation tools are needed. Also, the defective structure provides numerous crack sites and it becomes difficult to track and examine the cracking or delamination behaviour by conventional mechanical tests (e.g. tensile detachment, double or tapered double cantilever beam, peel resistance tests, pull-off test or blister tests), and especially where tight tolerances imposed in bonded structures are important.

There is no simple relationship between the structure of an adhesive based joint and its influence on degradation and failure during its potential applications [20]. However, this FE simulation work provides an ability to relate the role of the type of adhesively bonded structural combination and their relationships to degradation and failure, which otherwise would be difficult to ascertain using experimental techniques (e.g. in deflection based flexural investigation). These stress analysis findings can be incorporated in manufacturing adhesive joint specimens with desired properties and developing experimental framework under fully instrumented mechanical testing procedures [21-22] (e.g. acoustic emission, displacement and force transducer based 4-point bending, indentation or impact testing).

The quality and durability of such adhesive joint or structures has not been extensively characterized through simulation or experiments to date. Any future work therefore should address the prediction of durability of adhesive joints used for structural rehabilitation, and which can provide first step in the development of a procedure for assessment of reliability. It is anticipated that any enhanced evaluation methodologies should predict the adhesive joint strength (or residual strength for decommissioning industry) with high accuracy. Sensor based instrumented measurement and metrology (possibly combined test methodologies, both non-

destructive and semi-destructive) is an important proposition for future re-use or recycling of adhesive joint structures. Such structures can provide numerous failure sites and it may become difficult to track and examine the quality or residual strength by conventional standardized tests. Overall aim of any future framework model development should be developing novel diagnostic tool for enhanced characterisation of adhesive joints for re-use applications. To characterize the residual strength capability of a given adhesive joint structure under certain loading conditions, prediction techniques can be developed with a thorough understanding of the complexities involved in evaluating the residual strength. In multiple load path, built-up structures, whether classified as slow crack growth or fail-safe structures, the strength analysis can become complicated due to the complex geometric construction of the built-up components. In general, the prediction techniques are based on the critical value of the stress-intensity factor for a given geometry and loading.

Above proposition has considerable potential to assess the unique micromechanics within small volumes during mechanical testing and therefore to provide a means of evaluating the bond quality, with possible applications in test monitoring and quality control [23-24]. Despite some theoretical limitations (e.g. considering elastic–plastic deformable material, ignoring surface roughness, and taking adherends and adhesives as solid and homogeneous materials), the FE simulations of 4-point bending on metal-to-metal adhesive systems presents a good summary of the theoretical findings related to the observed stress profile. The mechanics investigated in this paper, however, are applicable to any flexural test configuration.

5. Conclusions

FE simulations of slender metal-to-metal adhesive joints have been investigated to understand the stress distributions along the thicknesses for two different adhesive types (brittle and ductile adhesives). It furthers the understanding of the behaviour of the sandwich joint in the context of the effect of the adherend stiffness on the adhesive layer stress state at various adhesive thicknesses thus highlighting the disparity in the joint strengths as a function of the adhesive modulus and thickness. The study has been conducted to understand if the stress states in the adhesive layer can be correlated to conventional bending theory so as to enable the effective design of a metal-adhesive sandwich specimen. It also highlights the effect of adherend plastic deformation on the adhesive layer stress state as a function of the adhesive layer thickness, including experimental validation. The key conclusions are as follows:

a. The adhesive thickness and modulus play an important role in determining flexibility and the load carrying capability of the adhesive joint. The effect of the modulus is not distinguishable at lower thicknesses of the adhesive layer, but increases with increasing thickness. The adhesive layer has some load carrying capability of its own which increases with increasing adhesive thickness and also the adhesive modulus.

b. The constraint exerted by the adherends limits the deformation of the adhesive layer especially at lower adhesive thicknesses, thus restricting the failure.

c. The stress states induced in the adhesive can also be explained by bi-material beam bending theory. The distance of the concerned layer (OA, OB or OC) from the corresponding neutral axis affects the stress state as both the stress state and the distance follow similar trend.

d. Although the mid-span shear stress values are consistently close to zero in both the brittle and ductile adhesives, the distribution is affected by the load concentration around the loading pin. The effect is more pronounced in the brittle adhesive, where steep changes in the shear stress distribution around the load point can be seen at higher thicknesses of the adhesive layer. At lower thicknesses, the adhesive layer is constrained by the adherends and hence the effects are localised around the load pin.

e. The stress distribution in all the combinations simulated is affected by the loading pin and to an extent by the support pin. The adhesive volume directly below the loading point is under a high degree of stress concentration and the stress changes its nature drastically in many of the cases considered. Hence this region may act as the failure initiation region.

f. The overall agreement between the FE simulation and the experimental results validate the simulation technique though the simulation slightly underestimates the load-carrying capability of the specimens in cases where there is no discernible failure of the adhesive layer.

References

[1] Higgins, A., Int. J. Adhes. Adhes. **20**, 367-376 (2000).

[2] Karachalios, E. F., Adams, R. D., and da Silva, L. F. M., J. Adhes. Sci. Technol. **27**, 1811-1827 (2013).

[3] Grant, L. D. R., Adams, R. D., and da Silva, L. F. M., Int. J. Adhes. Adhes. **29**, 405-413 (2009).

[4] Wisnom, M. R., and Cui, W. C., Comp. Sci. Technol. **45**, 323-334 (1992).

[5] Xie, M., and Adams, D. F., Compos. **26**, 653-659 (1995).

[6] Feraboli, P., and Ketward, K. T., Compos. Part A. **34**, 1265-1271 (2003).

[7] de Morais, A. B., and Pereira, A. B., Compos. Part A. **40**, 1741-1746 (2009).

[8] Sawa, T., Ichikawa, K., Shin, Y., and Kobayashi, T., Int. J. Adhes. Adhes. **30**, 298-305 (2010).

[9] Liu, J., Sawa, T., and Toratani, H., J. Adhes. **69**, 263-291 (1992).

[10] Kafkalidis, M. S., Thouless, M. D., Yang, Q.D., and Ward, S. M., J. Adhes. Sci. Technol. **14**, 1593-1607 (2000).

[11] LOCTITE. (2004) Loctite®326 [Online] Available from: http://www.farnell.com/datasheets/40157.pdf. [Accessed: 1 October 2014].

[12] Engineering Toolbox. [Online] Available from: http://www.engineeringtoolbox.com/young-modulus-d_417.html. [Accessed: 1 October 2014].

[13] Thouless, M. D., Adams, J. L., Kafkalidis, M. S., Ward, S. M., Dickie, R. A., and Westerbeek, G. L., J. Mater. Sci. **33**, 189-197 (1998).

[14] Yang, Q. D., Thouless, M. D., and Ward, S. M., J. Mech. Phys. Sol. **47**, 1337-1353 (1999).

[15] Tvergaard, V., and Hutchinson, J. W., J. Mech. Phys. Sol. **44**, 789-900 (1996).

[16] Marzi, S., Biel, A., and Stigh, U., Int. J. Adhes. Adhes. **31**, 840-850 (2011).

[17] Pardoen, T., Ferracin, T., Landis, C. M., and Delannay, F., J. Mech. Phys. Sol. **53**, 1951-1983 (2005).

[18] Naito, K., Onta, M., and Koga, Y., Int. J. Adhes. Adhes. **36**, 77-85 (2012).

[19] Xu, W., and Wei, Y., Int. J. Adhes. Adhes. **40**, 158-167 (2013).

[20] Choupani, N., Int. J. Adhes. Adhes. **28**, 267-282 (2008).

[21] Faisal, N. H., and Ahmed, R., Meas. Sci. Technol. **22**, 015703 (2011).

[22] Faisal, N. H., Ahmed, R., and Reuben, R. L., Int. Mater. Rev. **4**, 98-142 (2011).

[23] Faisal, N. H., Ahmed, R., Goel, S., and Fu, Y. Q., Surf. Coat. Technol. **242**, 42-53 (2014).

[24] Faisal, N. H., and Ahmed, R., Measur. Sci. Technol. **22**, 125704 (2011).

Figure 1. 4-point bending finite element simulation schemes for metal-to-metal adhesively bonded structure: (a) geometrical model, (b) axis symmetric half model, (c) meshing of the model and joint configuration, (d) paths OA, OB and OC in the adhesive, and (e) elastic-plastic deformed model shown here at the maximum loading pin displacement of 10 mm.

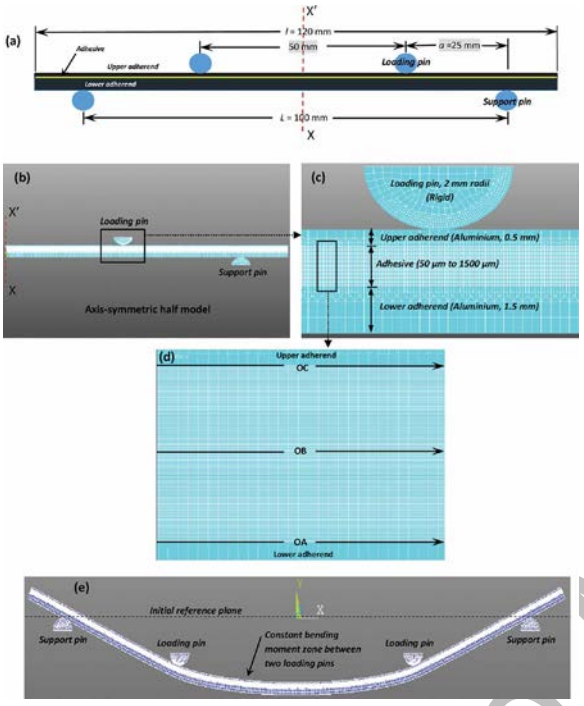

Figure 2. Traction-separation law of the CZM (adapted from ANSYS 14.0 documentation).

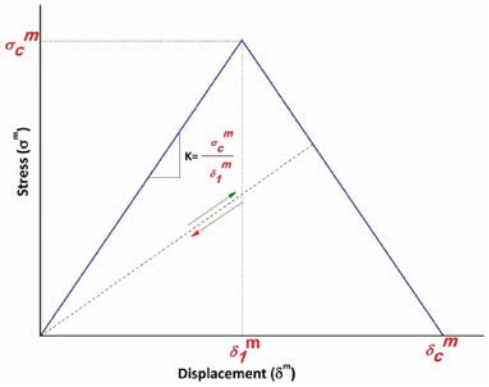

Figure 3. Metal-to-metal adhesive bond specimen preparation scheme.

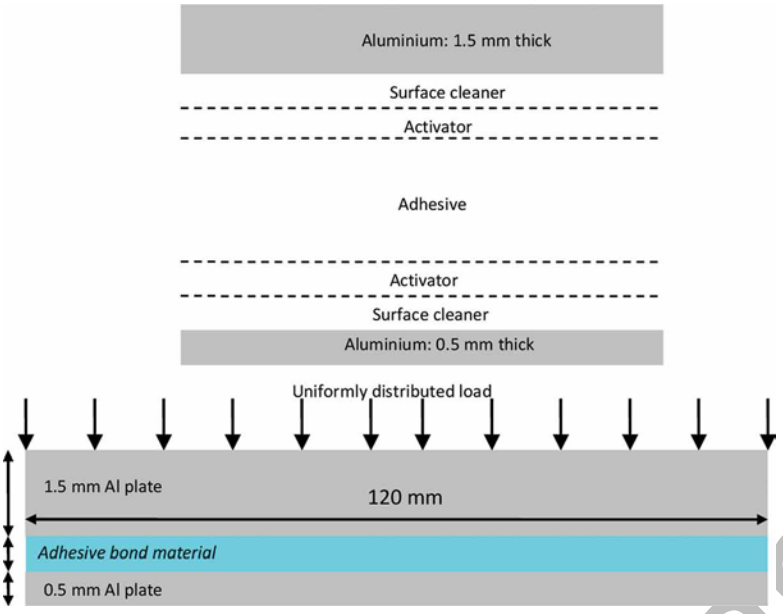

Figure 4. Normalised X-directional stress profile along OA, OB and OC with brittle adhesive: (a) 50 µm thick, and (b) 1500 µm thick, (c) along OA for all thicknesses, (d) along OB for all thicknesses, and (e) along OC for all thicknesses.

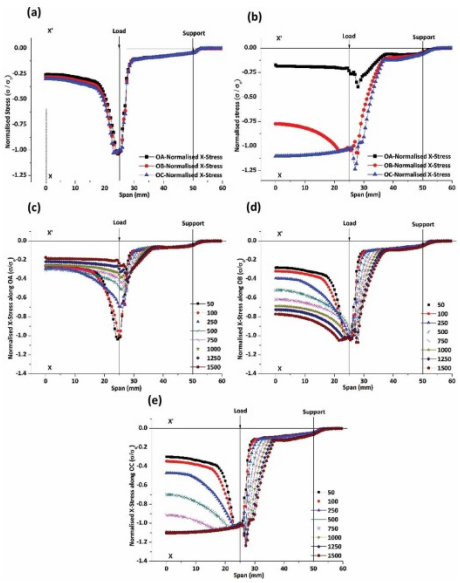

Figure 5. Normalised shear stress profile along OA, OB and OC with brittle adhesive: (a) 50 μm thick, and (b) 1500 μm thick, (c) along OA for all thicknesses, (d) along OB for all thicknesses, and (e) along OC for all thicknesses.

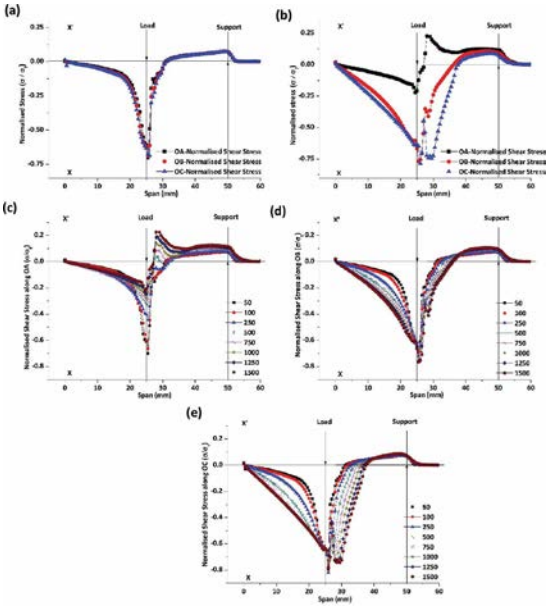

Figure 6. Normalised X-directional stress profile along OA, OB and OC with ductile adhesive: (a) 50 µm thick, and (b) 1500 µm thick, (c) along OA for all thicknesses, (d) along OB for all thicknesses, and (e) along OC for all thicknesses.

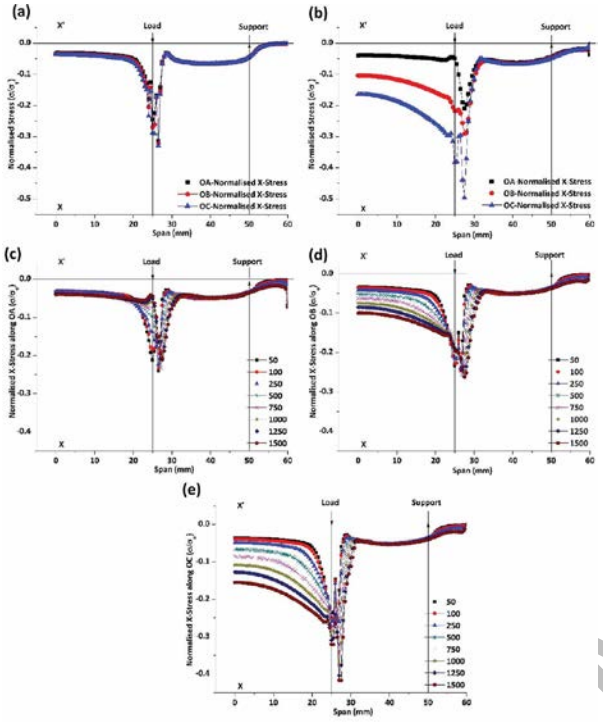

Figure 7. Normalised shear stress profile along OA, OB and OC with ductile adhesive: (a) 50 µm thick, and (b) 1500 µm thick, (c) along OA for all thicknesses, (d) along OB for all thicknesses, and (e) along OC for all thicknesses.

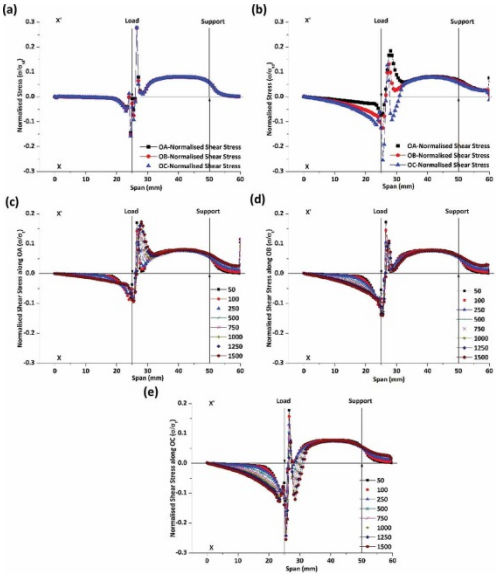

Figure 8**.** (a) Load vs thicknesses profiles of the brittle and ductile adhesives at a displacement of 10 mm, and (b) load vs displacement profiles of 50 µm and 1500 µm brittle and ductile adhesive layer joints.

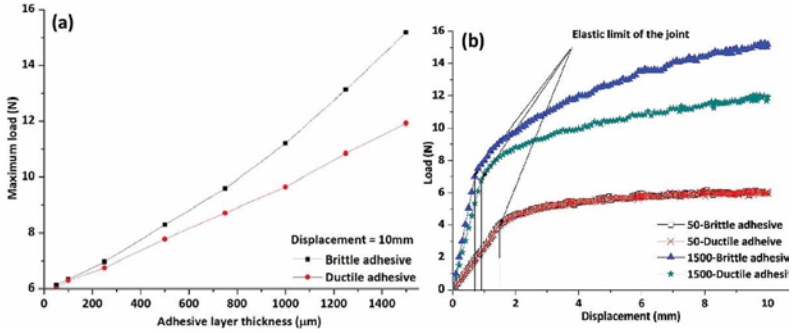

Figure 9. Comparison of stress profiles between brittle and ductile adhesive s along the path OA: (a) X-directional stress profile in 50 μm thick, (b) X-directional stress profile in 1500 μm thick, (c) shear stress profile in 50 μm thick, and (d) shear stress profile in 1500 μm thick.

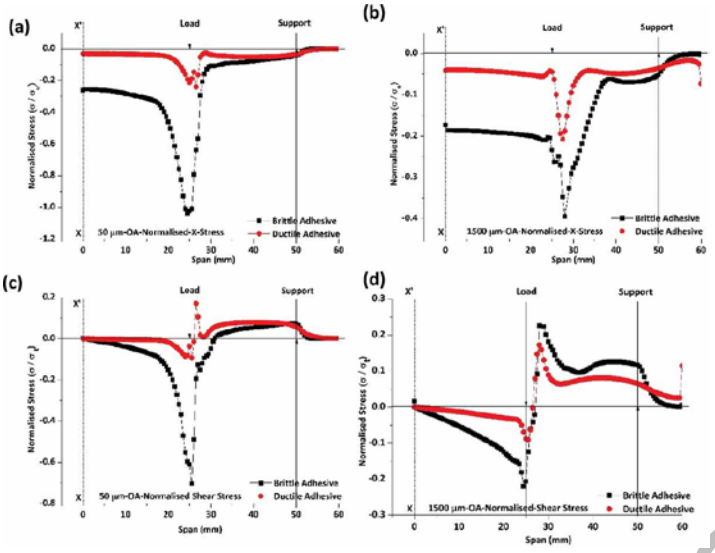

Figure 10. Mid-span normalised von-Mises stress vs adhesive layer thickness plots: (a) brittle adhesive, and (b) ductile adhesive.

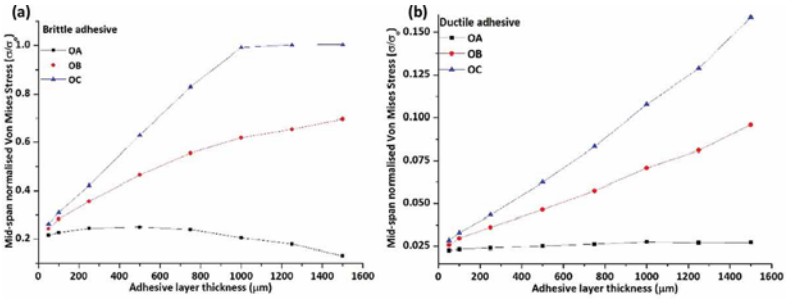

Figure 11. Distance of OA, OB and OC from neutral axis: (a) brittle adhesive, and (b) ductile adhesive.

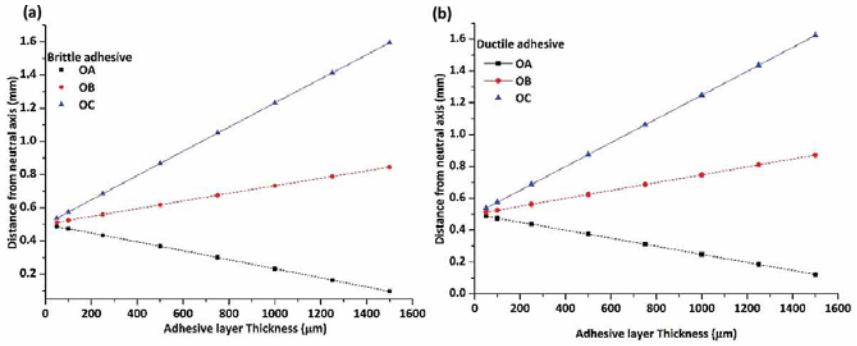

Figure 12. Experimental validation of FE model during 4-point bending: Comparison of force-displacement profile for *Al*-to-*Al* adhesively bonded specimens with brittle (Loctite® 3430™) and ductile (Loctite® 326™) adhesives of thicknesses 100 µm and 250 µm (CZM has been done in the model for 250 µm adhesive layer joints) [note: the force (y-axis) obtained from each test has been calculated per unit width of the specimen so as to be compared with the FE simulation force-displacement data].

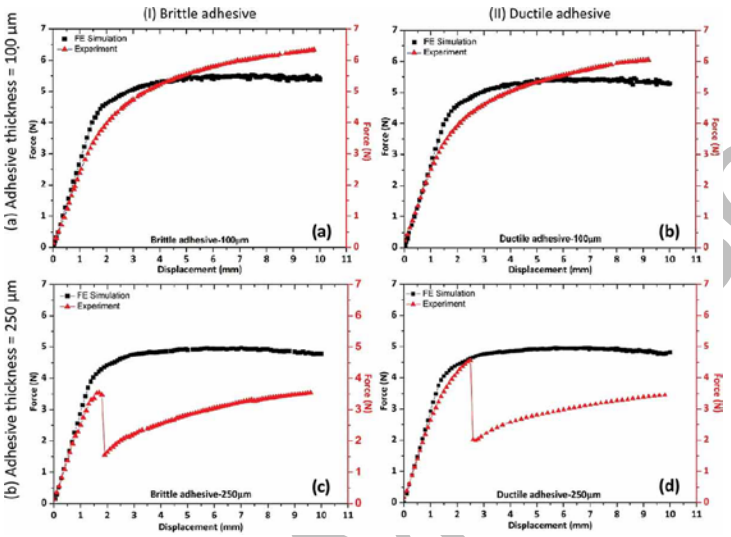

Table 1. Input parameters for finite element (FE) simulations.

Properties	**Young's modulus, *E* (GPa)**	**Poisson's ratio (*ν*)**	**Yield strength (MPa)**	**Tensile strength (MPa)**	**Length, *l* (mm)**	**Thickness, *t***
Lower adherend (aluminium)	68.4 [12]	0.3 [12]	105 [12]	116 [12]	120	1.5 mm
Upper adherend (aluminium)	68.4 [12]	0.3 [12]	105 [12]	116 [12]	120	0.5 mm
Brittle adhesive (Polyamide)	3.340 [8]	0.38 [8]	48.07 [8]	50.96 [8]	120	(50, 100, 250, 500, 750, 1000, 1250 and 1500) μm
Ductile adhesive (Acrylic)	0.300 [11]	0.2 [11]	34 [11]	45.3 [11]	120	(50, 100, 250, 500, 750, 1000, 1250 and 1500) μm